PHYSICAL REVIEW B **94**, 180408(R) (2016)

Interfacial control of Dzyaloshinskii-Moriya interaction in heavy metal/ferromagnetic metal thin film heterostructures

Xin Ma,[1] Guoqiang Yu,[2] Xiang Li,[2] Tao Wang,[3] Di Wu,[2] Kevin S. Olsson,[1] Zhaodong Chu,[1] Kyongmo An,[1] John Q. Xiao,[3] Kang L. Wang,[2] and Xiaoqin Li[1,*]

[1]*Department of Physics, Center for Complex Quantum Systems, The University of Texas at Austin, Austin, Texas 78712, USA*

[2]*Department of Electrical Engineering, University of California, Los Angeles, California 90095, USA*

[3]*Department of Physics and Astronomy, University of Delaware, Newark, Delaware 19716, USA*

(Received 14 July 2016; revised manuscript received 11 November 2016; published 28 November 2016)

The interfacial Dzyaloshinskii-Moriya interaction (DMI) in ultrathin magnetic thin film heterostructures provides a new approach for controlling spin textures on mesoscopic length scales. Here we investigate the dependence of the interfacial DMI constant D on a Pt wedge insertion layer in Ta/CoFeB/Pt(wedge)/MgO thin films by observing the asymmetric spin-wave dispersion using Brillouin light scattering. Continuous tuning of D by more than a factor of 3 is realized by inserting less than one monolayer of Pt. The observations provide new insights for designing magnetic thin film heterostructures with tailored D for controlling skyrmions and magnetic domain-wall chirality and dynamics.

DOI: 10.1103/PhysRevB.94.180408

I. INTRODUCTION

The Dzyaloshinskii-Moriya interaction (DMI) refers to an antisymmetric exchange interaction that promotes canted instead of the parallel or antiparallel spin alignments. Understanding and controlling the DMI may facilitate the design of the next-generation magnetic memory and logic devices based on chiral magnetic domain walls [1–5] and skyrmions [6–11]. Fast current-induced magnetic domain-wall motion has recently been demonstrated via the combination of a chiral domain-wall structure and spin-orbit torque where the direction and the speed of domain-wall motion depend on the sign, the strength of the DMI, and the spin-orbit torque [1,2]. Moreover, the DMI is responsible for establishing and controlling the sizes of magnetic skyrmions, which are topologically protected vortex- or hedgehoglike spin structures [7]. These small chiral spin textures show promise in future spintronic applications due to their unique properties including driven propagation by ultralow current densities [8,10,11] and rewritability by spin-polarized currents [6].

The magnitude of the DMI can be significant at the interface between a ferromagnetic metal (FM) and a nonmagnetic heavy metal (HM) possessing strong spin-orbit coupling. The enhanced DMI originates from the three-site indirect exchange interaction [12] and helps to stabilize the skyrmion bubble phase at room temperature [9,13–16]. Moreover, such an interfacial DMI in a multilayer heterostructure strongly depends on material composition, layer sequence, and interface quality among other factors [1,4,17–22]. This broad parameter space offers unique opportunities to elucidate the underlying physical origin of the interfacial DMI.

In this Rapid Communication, we demonstrate effective interfacial control of the DMI in annealed Ta/CoFeB/(Pt)/ MgO multilayers. The sign and magnitude of the DMI constant D are obtained from the asymmetric spin-wave dispersion probed with Brillouin light scattering (BLS). Continuous tuning of D by more than a factor of 3 is realized by inserting a Pt wedge with nominal thickness of less than one monolayer between the CoFeB and MgO layers. Both Ta/CoFeB and CoFeB/Pt interfaces contribute to the overall DMI but with different signs of D. The thicker region of the Pt wedge shows a larger magnitude of D at the CoFeB/Pt interface, leading a smaller net D value in the multilayer structure. This somewhat surprising finding of strong DMI strength modulation via an ultrathin Pt insertion layer together with magnetic anisotropy change in this multilayer heterostructure provides new approaches for controlling skyrmions and magnetic domain walls for new and emerging spintronic applications.

II. EXPERIMENTS

A series of Ta(5)/$Co_{20}Fe_{60}B_{20}$(1)/Pt(t_{Pt})/MgO(2)/Ta(2) thin films were deposited by magnetron sputtering at room temperature on thermally oxidized silicon substrates as shown in Fig. 1(a) where the numbers in parentheses represent the nominal layer thicknesses in nanometers. For one of the multilayer structures, the wedge-shape Pt-insert layer between the CoFeB and the MgO layers has the thickness variation from 0.11 to 0.29 nm across the 5-cm-long sample [13]. Following the deposition, all multilayer structures were annealed at 250° C for 30 min to enhance the perpendicular magnetic anisotropy.

BLS measurements were performed to investigate the asymmetric spin-wave dispersion caused by the interfacial DMI. Figure 1(b) shows the geometry of a BLS experiment where a magnetic-field **H** was applied along the z axis in all measurements. A s-polarized laser beam was incident on the sample, and the p-polarized component of the backscattered light was collected and sent to a Sandercock-type multipass tandem Fabry-Pérot interferometer. In order to reduce the uncertainty in k_M, a lens with a focal length of 10 cm was used to focus the incidence light and to collect the scattering signal. In addition, an aperture with a 5-mm diameter was placed near the lens as a spatial filter. In the light-scattering process, the total momentum is conserved on the plane of the thin film. As a result, the Stokes (anti-Stokes) peaks in BLS spectra correspond to the creation (annihilation) of magnons with momentum $k_M = \frac{4\pi}{\lambda} \sin\theta$ along the $-x$ ($+x$) direction as illustrated in Fig. 1(b), where $\lambda = 532$ nm is the laser

*elaineli@physics.utexas.edu

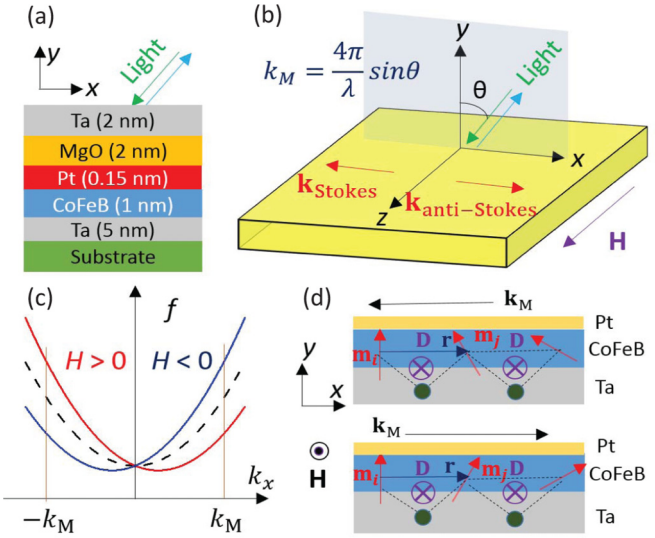

FIG. 1. Schematics of (a) a multilayer thin film and (b) BLS measurement geometry. (c) Spin-wave dispersions without (dashed line) and with (solid lines) the interfacial DMI $D > 0$. (d) Schematics of spatial chiralities of DE spin waves propagating in opposite directions. Canted red arrows $\mathbf{m}_i$ and $\mathbf{m}_j$ refer to the spin rotation on the x-y plane away from the external field direction $+z$ at different atomic sites i and j, respectively. The DMI vector $\mathbf{D}$ points into the paper plane ($D > 0$) for the two spins with spatial displacement $\mathbf{r}$. The green dots represent the Ta atoms, and the dashed line indicates the three-site indirect exchange.

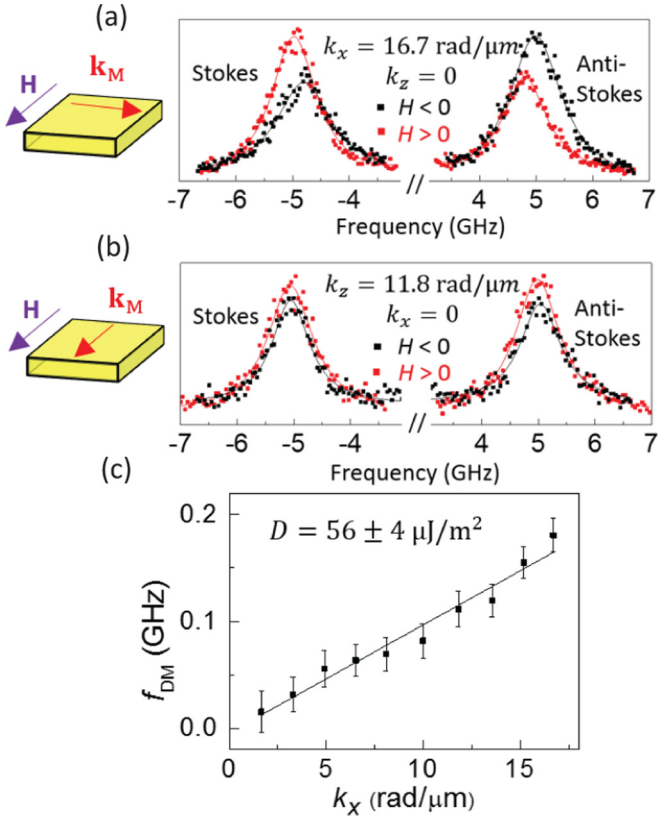

FIG. 2. BLS spectra for spin waves of (a) the DE mode and (b) the BWVM mode recorded at fixed incident angles under oppositely oriented external magnetic fields **H**. The solid lines represent fittings with Lorentzian functions. (c) The linear dependence of f_{DM} on k_x. The error bars on f_{DM} are determined from the deviation of Lorentzian fitting on BLS spectra, and the solid line refers to the least-squares fit. The uncertainty of D is estimated from the deviation of the least-squares fit.

wavelength and θ refers to the light incident angle. Owing to the presence of the DMI, shifts of spin-wave dispersions are introduced as displayed in Fig. 1(c). Such shifts are directly reflected in the frequency difference between the Stokes ($-k_M$) and the anti-Stokes (k_M) peaks in the BLS spectrum [17–20,22,23].

III. RESULTS AND DISCUSSION

The DMI influences spin-wave modes differently depending on their spin alignments. Two types of spin-wave modes are investigated here: (i) Damon-Eshbach (DE) modes propagating along the x axis perpendicular to the **H** direction [Fig. 1(d)], and (ii) backward volume (BWVM) modes propagating along the z axis parallel to the **H** direction. Figures 2(a) and 2(b) show typical BLS spectra for DE spin-wave modes and BWVM modes under opposite **H** directions on the Ta(5)/CoFeB(1)/Pt(0.15)/MgO thin films. In Fig. 2(a), both the intensities and the frequencies of the Stokes and the anti-Stokes peaks are asymmetric, whereas such asymmetric features can be interchanged by reversing the **H** direction. The intensity asymmetry originates from the surface propagating characteristics of DE spin waves [24]: higher (lower) intensity corresponds to the ones propagating near top (bottom) surface; the propagating direction of the DE spin waves ($\pm\mathbf{y} \times \mathbf{H}$) on each surface is reversed by opposite **H** directions. The frequency asymmetry is described by [19,20,25–27]

$$f = \frac{\gamma}{2\pi}\sqrt{\left(H + Jk_M^2\right)\left(H + Jk_M^2 + 4\pi M_{\text{eff}}\right)} - \text{sgn}(M_z)\frac{\gamma}{\pi M_S} D k_x, \quad (1)$$

when the magnetization is aligned along **H** in the thin film plane. Here γ is the gyromagnetic ratio $J = \frac{2A}{M_S}$ with the exchange stiffness constant A and the saturation magnetization M_S, k_x denotes the projection of k_M in the x direction, and $4\pi M_{\text{eff}} = 4\pi M_S - H_\perp$ represents the effective demagnetization field including the influence of interfacial magnetic anisotropy field described by $H_\perp$. The first term on the right describes the spin-wave dispersion without the DMI in the ultrathin film limit, and the second term accounts for the DMI. In Eq. (1), D, k_x, and $4\pi M_{\text{eff}}$ can be positive or negative values in the formula. f is different for $k_x < 0$ (Stokes) and $k_x > 0$ (anti-Stokes), leading to the frequency asymmetry. Specifically, the DMI reduces the energy and frequency of the spin waves with clockwise spatial chirality [e.g., $k_x > 0$ in Fig. 1(d) (bottom)] but increases the energy and frequency of those with counterclockwise spatial chirality [e.g., $k_x < 0$ in Fig. 1(d) (top)] if looking along the vector of **D** [18]. When the magnetic field is reversed, the direction of **D** remains the same, but the spatial chirality of spin waves interchange in k space between $k_x < 0$ (Stokes) and $k_x > 0$ (anti-Stokes). Thus the asymmetry in the spin-wave dispersion is reversed along the k_x direction as illustrated in Fig. 1(d) and demonstrated in Fig. 2(a). In contrast, such

intensity and frequency asymmetries are not observed for the BWVM spin waves shown in Fig. 2(b), owing to their bulk characteristics and the lack of the spatial chiralities $[-\mathbf{D}\cdot(\mathbf{m}_i\times\mathbf{m}_j)\neq 0]$ present in the DE modes. We note that the observed frequency asymmetry in Fig. 2(a) is not due to the nonreciprocity of the DE spin waves at the two surfaces [24,28,29] because $|k_x t(\mathrm{CoFeB})|\ll 1$ as discussed in Refs. [18,20]. Instead, it can be explained by the interfacial DMI.

In order to quantify the interfacial DMI constant D, momentum-resolved BLS measurements were performed through varying the incident angle [30]. According to Eq. (1), a linear correlation exists between $f(-k_x)-f(k_x)$ and k_x where the slope is determined by D [23,31]. To further avoid possible instrument frequency offsets in the frequency difference between Stokes and anti-Stokes peaks, we subtract the values obtained by reversing the applied $\mathbf{H}$ field as described by the following equation:

$$f_{\mathrm{DM}}=\frac{\{[f(-k_x,M_z)-f(k_x,M_z)]-[f(-k_x,-M_z)-f(k_x,-M_z)]\}}{2}=\frac{2\gamma}{\pi M_{\mathrm{S}}}Dk_x. \tag{2}$$

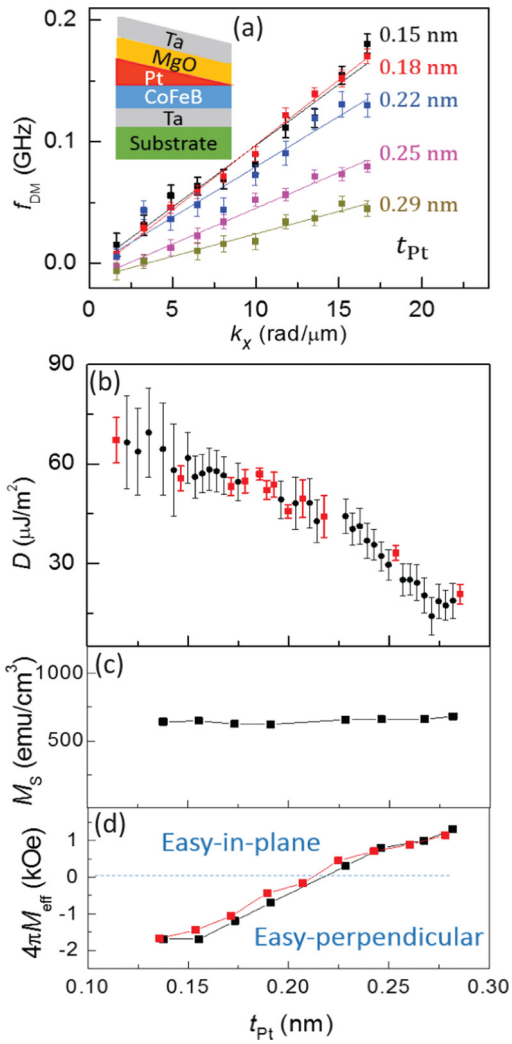

FIG. 3. (a) The linear dependences of f_{DM} on k_x for a Pt wedge layer with a thickness gradient where the inset illustrates the multilayer structure. The solid lines show the least-squares fits. (b) The interfacial DMI constant D as a function of the Pt layer thickness t_{Pt}. The red squares are derived from the linear fits on the k_x dependences of f_{DM} with different t_{Pt}'s using Eq. (2). The black circles are obtained through f_{DM}/k_x at fixed $k_x=16.7$ rad/μm by varying t_{Pt} in a smaller step size. (c) M_{S} and (d) $4\pi M_{\mathrm{eff}}$ as functions of t_{Pt}. The red (black) dots in (d) are obtained from the field dependence BLS (VSM) measurements, respectively.

Figure 2(c) plots the DMI-induced frequency shift f_{DM} as a function of k_x for the Ta(5)/CoFeB(1)/Pt(0.15)/MgO thin film, which can be fitted linearly. Considering $\gamma=17.6$ GHz/kOe and taking $M_{\mathrm{s}}=640$ emu/cm^3 obtained from vibrating sample magnetometer (VSM) measurements, $D=56\pm 4\ \mu\mathrm{J/m^2}$ is determined from the slope of the linear correlation. We note that the D value here is modest compared with that in the Pt/FM systems [19,20,22,23,31]. Nevertheless, the DMI on the annealed Ta/CoFeB structures is still of great interest for the study of skyrmions. The enhanced interfacial magnetic anisotropy field $H_\perp$ in our sample compensates the demagnetization field in thin films and brings $4\pi M_{\mathrm{eff}}$ close to zero, a condition favorable for establishing room-temperature skyrmions [13].

To control the DMI and to elucidate the role of the Pt layer, a wedged Pt layer was inserted between the CoFeB and the MgO layers. Therefore, a spatial gradient in the DMI is introduced. The k_x-dependent BLS spectra at different positions on the heterostructures correspond to different Pt thicknesses [Fig. 3(a)]. The influence of the Pt wedge on M_{s} is negligibly small as shown in Fig. 3(c). Thus, according to Eq. (2), the observed change in the slope [Fig. 3(a)] mainly originates from the change in the D value. D is found to vary by more than a factor of 3 when the nominal Pt thickness varies from 0.11 to 0.29 nm as shown in Fig. 3(b). We note that the magnetic anisotropy also gradually changes with the increasing Pt thickness as determined from the field dependence BLS and VSM results, see the Supplemental Material [32] [Fig. 3(d)]. This is owing to the fact that Pt atoms weaken the Co-O and Fe-O bonds at the interface between CoFeB and MgO [13]. This change in magnetic anisotropy may lead to a slight underestimation in the modification of D, see the Supplemental Material [32].

In our sample, both the bottom Ta/CoFeB and the top CoFeB/Pt interfaces contribute to the DMI but partially cancel each other. The DMI vector for two spins with spatial displacement $\mathbf{r}$ can be written as $\mathbf{D}_{\mathrm{Ta(Pt)}}=D_{\mathrm{Ta(Pt)}}\mathbf{n}_{\mathrm{Ta(Pt)}}\times\mathbf{r}/r$, where $\mathbf{n}_{\mathrm{Ta(Pt)}}$ denotes the unit vector pointing from Ta(Pt) to CoFeB and $\mathbf{n}_{\mathrm{Ta}}=-\mathbf{n}_{\mathrm{Pt}}$ as illustrated in Fig. 4(a). Although the spin Hall angles of Ta and Pt are opposite, the $D_{\mathrm{Ta(Pt)}}$'s induced by Pt and Ta on ferromagnetic metals have the same sign [2,21]. Assuming that $\mathbf{r}=\mathbf{x}$ and $D_{\mathrm{Ta(Pt)}}>0$, $\mathbf{D}_{\mathrm{Ta(Pt)}}$ induced from the bottom Ta (top Pt) layer lies in the $-z$ ($+z$) direction owing to the opposite directions of $\mathbf{n}_{\mathrm{Ta(Pt)}}$ [Fig. 4(a)]. As the Pt layer becomes thicker, more Pt atoms contribute to the DMI and

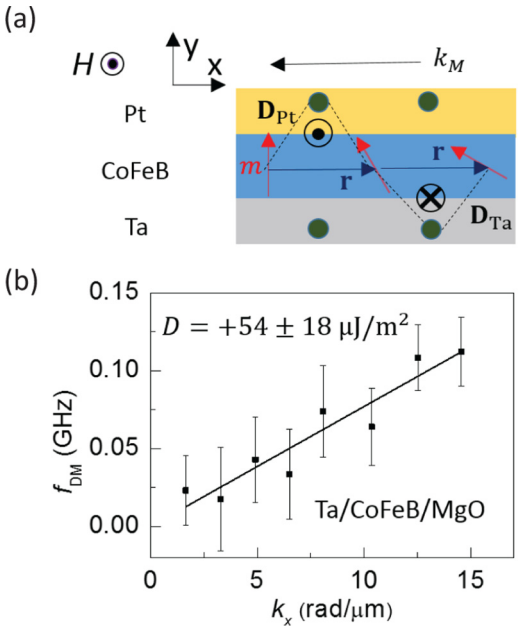

FIG. 4. (a) Schematics of the directions of $\mathbf{D}_{Ta}$ (pointing along $-z$) and $\mathbf{D}_{Pt}$ (pointing along $+z$) on annealed Ta/CoFeB/Pt/MgO. The green dots represent the HM atoms. (b) The linear dependence of f_{DM} on k_x extracted from a control sample, annealed Ta(5)/CoFeB(1.1)/MgO.

hence partially compensate the DMI initially established by the bottom Ta layer. Moreover, a very small amount of Pt is sufficient to effectively compensate the DMI introduced by the Ta layer because the D_{Pt} induced by Pt is much stronger than the D_{Ta} induced by Ta [1,2,4,22].

Next, we discuss that the positive sign of D found in our Ta(5)/CoFeB(1)/Pt(wedge)/MgO structures may be related to specific atomic arrangements at the HM/FM interface. In order to exclude the impact of the Pt layer in Fig. 3(a), BLS studies were performed on a control sample Ta(5)/CoFeB(1.1)/MgO with the same growth condition. Figure 4(b) shows that this particular control sample Ta(5)/CoFeB(1.1)/MgO also exhibits a positive D (right-handed magnetic chirality), whereas negative D values have been reported by other groups in similar HM/FM structures, such as Pt/CoFe and Pt/Co [2,14,19]. We speculate that the diffusion of B atoms in CoFeB during annealing causes the change in D. It has been shown that B atoms diffuse towards the interface during the annealing procedure and modify the relative positions of FM and HM atoms at CoFeB/heavy metal interfaces [21], which in turn is expected to lead to a modified DMI. In addition, a strong accumulation of B in the bottom Ta layer may affect the electronegativity of the heavy metal layer and hence reverse the sign of D. Our speculation is supported by previous studies in which a nitrogen-doped-Ta/CoFeB structure is shown to exhibit opposite DMI constants compared with a pure-Ta/CoFeB system [4]. A similar effect has also been observed on annealed Ta/CoFeB and Pt/CoFeB structures through the domain-wall studies by us and others [21,33], where D becomes positive.

Finally, we note that the D value of the Ta(5)/CoFeB(1.1)/MgO sample in Fig. 4(b) is slightly smaller than that of Ta(5)/CoFeB(1)/Pt(wedge)/MgO in Fig. 3(b) in the limit of zero Pt thickness. There are some variations between the samples that contributed to this apparent difference. First the thickness of the magnetic layer (CoFeB) is different, leading to an expected reduction in D for the control sample Ta(5)/CoFeB(1.1)/ MgO. Previous studies have shown that D is roughly linearly dependent on $1/t_{FM}$, despite some deviation in the ultrathin region [17,18]. In addition, there might be small variance in D values among different samples as it is highly sensitive to the interface quality [22].

IV. CONCLUSION

In conclusion, we demonstrate effective interfacial control of the DMI on annealed Ta/CoFeB/(Pt)/MgO multilayer thin films where the overall DMI strength results from the additive effect of both the Ta/CoFeB and the CoFeB/Pt interfaces. Continuous tuning of the DMI constant D by more than a factor of 3 is realized via less than one monolayer of Pt insertion in between the CoFeB and the MgO layers. The larger net D occurs at positions with the thinner Pt wedge, and the final sign of D is determined by the Ta layer. Our results demonstrate that the use of two HM-, DMI-active layers provides an efficient way for DMI control in the magnetic multilayers. Our Rapid Communication suggests that simultaneous enhancement of D and the reduction of magnetic anisotropies can be realized by choosing HM materials and their thicknesses properly. This flexibility in materials properties engineering may enable skyrmions with nanometer dimensions at room temperature, which is highly desirable for high-density spintronic applications.

ACKNOWLEDGMENTS

The work at UT-Austin and UCLA was supported by SHINES, an Energy Frontier Research Center funded by the U.S. Department of Energy (DoE), Office of Science, Basic Energy Science (BES) under Award No. DE-SC0012670. The work at the University of Delaware was supported by NSF DMR Grant No. 1505192.

[1] K.-S. Ryu, L. Thomas, S.-H. Yang, and S. Parkin, Nat. Nanotechnol. **8**, 527 (2013).

[2] S. Emori, U. Bauer, S.-M. Ahn, E. Martinez, and G. S. D. Beach, Nature Mater. **12**, 611 (2013).

[3] G. Chen, T. Ma, A. T. N'Diaye, H. Kwon, C. Won, Y. Wu, and A. K. Schmid, Nat. Commun. **4**, 2671 (2013).

[4] J. Torrejon, J. Kim, J. Sinha, S. Mitani, M. Hayashi, M. Yamanouchi, and H. Ohno, Nat. Commun. **5**, 4655 (2014).

[5] S. Pizzini, J. Vogel, S. Rohart, L. D. Buda-Prejbeanu, E. Jué, O. Boulle, I. M. Miron, C. K. Safeer, S. Auffret, G. Gaudin, and A. Thiaville, Phys. Rev. Lett. **113**, 047203 (2014).

[6] N. Romming, C. Hanneken, M. Menzel, J. E. Bickel, B. Wolter, K. von Bergmann, A. Kubetzka, and R. Wiesendanger, Science **341**, 636 (2013).

[7] N. Nagaosa and Y. Tokura, Nat. Nanotechnol. **8**, 899 (2013).

[8] T. Schulz, R. Ritz, A. Bauer, M. Halder, M. Wagner, C. Franz, C. Pfleiderer, K. Everschor, M. Garst, and A. Rosch, Nat. Phys. **8**, 301 (2012).

[9] W. Jiang, P. Upadhyaya, W. Zhang, G. Yu, M. B. Jungfleisch, F. Y. Fradin, J. E. Pearson, Y. Tserkovnyak, K. L. Wang, O. Heinonen, S. G. E. te Velthuis, and A. Hoffmann, Science **349**, 283 (2015).

[10] J. Iwasaki, M. Mochizuki, and N. Nagaosa, Nat. Nanotechnol. **8**, 742 (2013).

[11] A. Fert, V. Cros, and J. Sampaio, Nat. Nanotechnol. **8**, 152 (2013).

[12] A. Fert and P. M. Levy, Phys. Rev. Lett. **44**, 1538 (1980).

[13] G. Yu, P. Upadhyaya, X. Li, W. Li, S. K. Kim, Y. Fan, K. L. Wong, Y. Tserkovnyak, P. K. Amiri, and K. L. Wang, Nano Lett. **16**, 1981 (2016).

[14] S. Woo, K. Litzius, B. Kruger, M.-Y. Im, L. Caretta, K. Richter, M. Mann, A. Krone, R. M. Reeve, M. Weigand, P. Agrawal, I. Lemesh, M.-A. Mawass, P. Fischer, M. Klaui, and G. S. D. Beach, Nature Mater. **15**, 501 (2016).

[15] G. Chen, A. Mascaraque, A. T. N'Diaye, and A. K. Schmid, Appl. Phys. Lett. **106**, 242404 (2015).

[16] O. Boulle, J. Vogel, H. Yang, S. Pizzini, D. de Souza Chaves, A. Locatelli, T. O. Menteş, A. Sala, L. D. Buda-Prejbeanu, O. Klein, M. Belmeguenai, Y. Roussigné, A. Stashkevich, S. M. Chérif, L. Aballe, M. Foerster, M. Chshiev, S. Auffret, I. M. Miron, and G. Gaudin, Nat. Nanotechnol. **11**, 449 (2016).

[17] J. Cho, N.-H. Kim, S. Lee, J.-S. Kim, R. Lavrijsen, A. Solignac, Y. Yin, D.-S. Han, N. J. J. van Hoof, H. J. M. Swagten, B. Koopmans, and C.-Y. You, Nat. Commun. **6**, 7635 (2015).

[18] H. T. Nembach, J. M. Shaw, M. Weiler, E. Jue, and T. J. Silva, Nat. Phys. **11**, 825 (2015).

[19] M. Belmeguenai, J.-P. Adam, Y. Roussigné, S. Eimer, T. Devolder, J.-V. Kim, S. M. Cherif, A. Stashkevich, and A. Thiaville, Phys. Rev. B **91**, 180405 (2015).

[20] K. Di, V. L. Zhang, H. S. Lim, S. C. Ng, M. H. Kuok, J. Yu, J. Yoon, X. Qiu, and H. Yang, Phys. Rev. Lett. **114**, 047201 (2015).

[21] R. Lo Conte, E. Martinez, A. Hrabec, A. Lamperti, T. Schulz, L. Nasi, L. Lazzarini, R. Mantovan, F. Maccherozzi, S. S. Dhesi, B. Ocker, C. H. Marrows, T. A. Moore, and M. Kläui, Phys. Rev. B **91**, 014433 (2015).

[22] N.-H. Kim, D.-S. Han, J. Jung, J. Cho, J.-S. Kim, H. J. M. Swagten, and C.-Y. You, Appl. Phys. Lett. **107**, 142408 (2015).

[23] K. Di, V. L. Zhang, H. S. Lim, S. C. Ng, M. H. Kuok, X. Qiu, and H. Yang, Appl. Phys. Lett. **106**, 052403 (2015).

[24] R. E. Camley, Surf. Sci. Rep. **7**, 103 (1987).

[25] J.-H. Moon, S.-M. Seo, K.-J. Lee, K.-W. Kim, J. Ryu, H.-W. Lee, R. D. McMichael, and M. D. Stiles, Phys. Rev. B **88**, 184404 (2013).

[26] S. Rohart and A. Thiaville, Phys. Rev. B **88**, 184422 (2013).

[27] A. N. Bogdanov and U. K. Rößler, Phys. Rev. Lett. **87**, 037203 (2001).

[28] G. Chen, J. Zhu, A. Quesada, J. Li, A. T. N'Diaye, Y. Huo, T. P. Ma, Y. Chen, H. Y. Kwon, C. Won, Z. Q. Qiu, A. K. Schmid, and Y. Z. Wu, Phys. Rev. Lett. **110**, 177204 (2013).

[29] M. Suzuki, H. Muraoka, Y. Inaba, H. Miyagawa, N. Kawamura, T. Shimatsu, H. Maruyama, N. Ishimatsu, Y. Isohama, and Y. Sonobe, Phys. Rev. B **72**, 054430 (2005).

[30] Z. K. Wang, V. L. Zhang, H. S. Lim, S. C. Ng, M. H. Kuok, S. Jain, and A. O. Adeyeye, Appl. Phys. Lett. **94**, 083112 (2009).

[31] V. L. Zhang, K. Di, H. S. Lim, S. C. Ng, M. H. Kuok, J. Yu, J. Yoon, X. Qiu, and H. Yang, Appl. Phys. Lett. **107**, 022402 (2015).

[32] See Supplemental Material at http://link.aps.org/supplemental/10.1103/PhysRevB.94.180408 for detailed results and analysis on field dependence BLS and VSM.

[33] G. Yu, P. Upadhyaya, K. L. Wong, W. Jiang, J. G. Alzate, J. Tang, P. K. Amiri, and K. L. Wang, Phys. Rev. B **89**, 104421 (2014).